EES Catalysis

PAPER

View Article Online
View Journal

Cite this: DOI: 10.1039/d6ey00012f

Low-frequency electrochemical pulsing to manage flooding and salt precipitation in zero-gap CO_2-to-ethylene electrolyzers

Michell Marufu,†[ad] Maxwell Goldman, †*[ad] R. Dominic Ross, †[ad] Jongmin Lee,[b] Jack Davis, [c] Michael Troksa,[c] Eric Krall,[a] Auston Clemens,[cd] Aditya Prajapati, [ad] Andrew A. Wong, [cd] Pavel Trtik,[b] Po-Ya Abel Chuang, [e] Eric B. Duoss, [c] Sarah E. Baker[ad] and Christopher Hahn *[ad]

Received 14th January 2026,
Accepted 27th January 2026

DOI: 10.1039/d6ey00012f

rsc.li/eescatalysis

The electrochemical reduction of carbon dioxide (CO_2) to ethylene presents a promising route for utilizing exhaust gases to produce value-added chemicals with broad manufacturing applications. While zero-gap electrolyzer architectures show great potential to enable commercial-scale CO_2-to-ethylene conversion, their performance is often limited by failure within the first 100 hours. In this work, we demonstrate that a low-frequency electrochemical pulsing protocol effectively mitigates carbonate salt precipitation and flooding by managing water transport to and through the cathode gas diffusion electrode and associated flow fields. *Operando* neutron imaging further reveals the dynamics of water crossover and flooding, emphasizing the intricate interplay between electrochemical operation and ionic transport. By mitigating short-term flooding and salt precipitation failure modes, this study establishes a foundation for understanding long-term degradation mechanisms and advancing the practical viability of CO_2 electrolyzers for industrial-scale applications.

Broader context

The electrochemical conversion of CO_2 to ethylene offers a promising approach to expand manufacturing of commodity chemicals and fuels. Specifically, ethylene is a critical precursor for polyethylene a $240B industry. Expanding productivity at existing ethylene plants would allow for rapid growth in the sector while alleviating the time delay associated with building new refineries. Energy efficient and durable CO_2 electrolysis to ethylene poses significant challenges because it requires a multistep reaction for C–C coupling, leading to multiple reaction products such as carbon monoxide, acetate, formate and ethanol. Our research addresses two short-term failure mechanisms of zero-gap CO_2 electrolysis to ethylene, namely salt precipitation, and catalyst flooding, which prevent industrial adoption. We show that a low frequency current pulsing protocol can manage water movement within the electrolyzer. These relaxation pulses allow for the dissolution of precipitated salts and for liquid organic byproducts to be removed from the cathode allowing for increase durability of the electrolyzer.

Introduction

Recent technological advancements in zero-gap electrolyzers have enabled the conversion of CO_2 into a variety of carbon-based chemical products, such as carbon monoxide (CO), methane (CH_4), and ethylene (C_2H_4).[1,2] However, the poor long-term stability of CO_2 electrolyzers remains a major barrier to their industrial adoption.[3–5] Over short operating time scales (<100 hours), the primary failure mechanisms are flooding and salt precipitation, which hinder CO_2 transport and obscure the study of longer-term failure mechanisms, such as catalyst deactivation, loss of cathode hydrophobicity, and component degradation.[6] In particular, achieving stable ethylene production at industrially relevant current densities (*i.e.* $\geq$200 mA cm^{-2}) has proven challenging, with operational lifetimes typically an order of magnitude shorter than those observed for CO_2 electrolysis to CO.[4] Understanding the causes of these early failure modes and developing materials and operational procedures to mitigate them are essential steps toward realizing durable, industrially relevant CO_2-to-ethylene electrolyzers.

[a] *Materials Science Division, Lawrence Livermore National Laboratory, 7000 East Avenue, Livermore, CA, 94550, USA. E-mail: goldman23@llnl.gov, hahn31@llnl.gov*
[b] *PSI Center for Neutron and Muon Sciences, 5232 Villigen PSI, Switzerland*
[c] *Materials Engineering Division, Lawrence Livermore National Laboratory, 7000 East Avenue, Livermore, CA, 94550, USA*
[d] *Laboratory for Energy Applications for the Future (LEAF), Lawrence Livermore National Laboratory, Livermore, CA, 94550, USA*
[e] *Department of Mechanical and Aerospace Engineering, University of California, Merced, CA 95343, USA*
† First authors.

Electrochemical current pulsing has been utilized for CO_2 electrolysis as a method for steering product selectivity and improving durability.[7,8] By changing the duration and magnitude of the pulses, physical and chemical mechanisms can be controlled, modifying the performance and durability of electrolyzers. Examples for CO_2 electrolysis include control of adsorbates (microseconds to milliseconds timescale), generation of diffusion gradients in solution (milliseconds to tens of seconds timescale), and control over catalyst speciation (seconds to minutes timescale). Some reports have demonstrated pulsed electrolysis at high frequencies (microseconds to second) to modify the catalyst surface at the atomic level to favor adsorption of CO and the rate of C–C coupling, resulting in increased faradaic efficiencies for specific carbon dioxide reduction reaction (CO_2RR) products.[9–11] Multiphysics simulations have demonstrated that during mid frequency current pulsing (10 s of seconds), dissolved CO_2 can accumulate at the catalyst triple phase boundary, and alter the local pH, thereby improving faradaic efficiency for C_{2+} products by suppressing the hydrogen evolution reaction (HER).[8,12,13] Low-frequency current pulsing (on the order of minutes) has been investigated for catalyst regeneration through oxidative pulses in zero-gap electrolyzers and in H-cells on copper sheets,[14,15] however, the impact of low-frequency pulses on transport phenomena has not been thoroughly explored for Cu-based catalysts in zero-gap electrolyzers. Current pulses on the timeframe of minutes have the potential to enhance electrolyzer durability by facilitating the flux of cations, liquid organic products and water throughout the membrane electrode assembly. By introducing step changes in the applied current density, this method allows relaxation periods for diffusion and transport processes to occur. These relaxation periods offer an opportunity to mitigate carbonate salt mitigation through humidity, decreased water consumption and reduction in hydroxide generation and simultaneously these relaxation steps may facilitate removal of hygroscopic liquid organic products from the electrode. Effectively these low frequency reduced current steps offer a unique opportunity to mitigate or slow down multiple failure modes for CO_2RR for C_{2+} products.[16] However, the underlying mechanisms governing the interaction between low-frequency pulsed currents and the transport phenomena of water and alkali cations remain poorly understood. This knowledge gap has hindered the broader adoption of pulsing strategies to extend the operational lifetime of CO_2 electrolyzers.

Systematic development of operational protocols for mitigating flooding and salt precipitation is hindered by a poor understanding of how different protocols affect water diffusion within the electrolyzer, which leads to each of these failure modes. Various approaches have been developed for the observation of water crossover in CO_2 electrolysis, but typically either provides insufficient field of view, time resolution, or otherwise severely compromises the geometry of the electrolyzer. Acrylic viewing windows on the flow fields have been used to observe salt precipitation and flooding at the back of the GDE in real time. However, this approach provides only a limited perspective and cannot capture through-plane water and cation transport before water breakthrough or salt precipitation becomes visible at the back of the GDE.[17] Wide angle X-ray scattering has also been used as a method to more completely study cation and water diffusion, which allows for observation of electro-osmotic diffusion of water and cations but requires a small cell size to accommodate the large attenuation of X-rays by the cell materials.[18,19] Additionally, only a relatively small area around the membrane can be imaged, but still requires acquisition times on the order of minutes. In contrast, *operando* neutron radiography (NR) allows us to glimpse into the transport phenomena over a wide field of view including both sets of flow fields. This technique takes advantage of the low attenuation of neutrons through metals and the high attenuation of neutrons through water.[20,21] However, only a limited number of operating conditions have been systematically investigated and rationally understood using insights from *operando* NR, especially for CO_2-to-ethylene conversion.

In this work, we employed a low frequency electrochemical current pulsing protocol on the minutes timescale to enable the humidified inlet CO_2 to dissolve carbonate salts formed within the flow field and gas diffusion layer. This step-based electrochemical pulsing is characterized by a "primary operational current density" (J_P), a lower "reduced current density" (J_R), and a periodic time interval for each t_P and t_R (Fig. 1b). We postulated that J_R would sufficiently slow down both the chemical reaction of CO_2 with OH^- to form (bi)carbonate and the electrochemical reaction of CO_2 which generates OH^-, to allow for the dissolution of precipitated salts at the cathode with the humidified CO_2 stream. We also aimed to find the ideal t_P that would maximize the rate of ethylene production while avoiding precipitation to the level that would cause electrolyzer failure. Using *operando* NR, we observed that our optimized low-frequency pulsing protocol allowed water to pass through the GDE and clear hygroscopic liquid products and salt through the flow fields. We present a systematic roadmap for developing a targeted mitigation strategy to simultaneously address precipitation and flooding, critical early failure modes, offering a framework that can be adapted and tailored to various electrolyzer configurations. Because each pulsing protocol is highly sensitive to material selection, any modification to system components often requires corresponding adjustments to the operating conditions. Therefore, establishing a well-defined and systematic methodology for protocol development will provide a valuable framework for advancing research and optimizing process control, ultimately bridging a critical gap in the development of pulsed-current strategies.

Results and discussion

As a starting point for high CO_2 to ethylene activity, we adopted an electrode designed based on previous optimization using Cu/ionomer nanoparticle overlayers for zero-gap electroreduction of CO_2 to ethylene. This design incorporates a Cu layer deposited through physical vapor deposition with an additional Cu-nanoparticle/ionomer layer on top. We previously identified that the additional nanoparticle/ionomer layer can improve

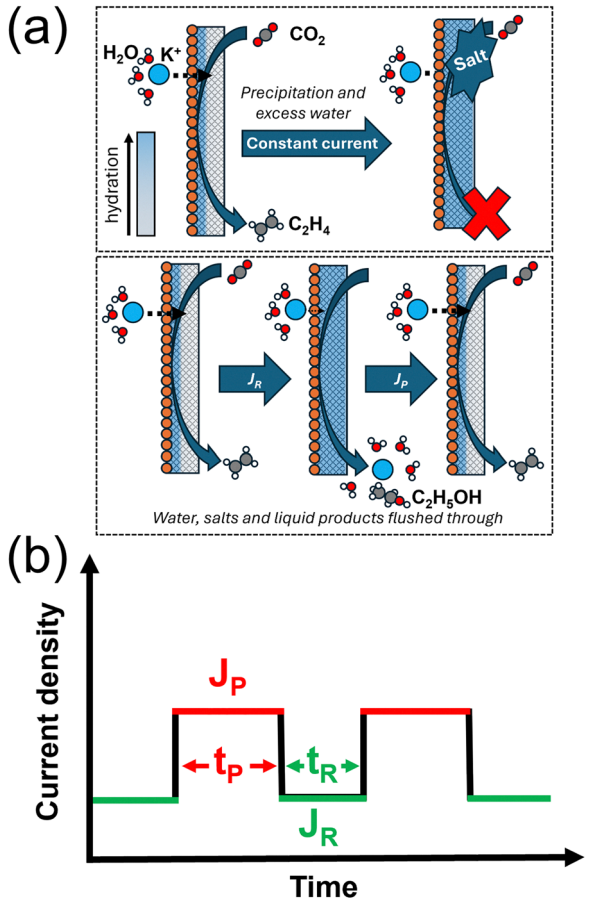

Fig. 1 Schematics of pulsed CO_2 electrolysis (a) Top: Cartoon depicting salt precipitation during constant current electrolysis, bottom: Cartoon depicting pulsed currents allowing water and salt to clear the electrolyzer. (b) General schematic of electrochemical pulsing at primary current density (J_P) and a reduced current density (J_R), and their corresponding times (t_P and t_R respectively). Blue coloring in the GDL represents a water filled GDL and grey represents a dry GDL, Blue circles represent K^+. The current remains cathodic throughout the experiment.

performance by tuning the water activity and mitigating electrolyzer flooding.[22] This work demonstrated that the TMA-PPO had superior activity ethylene production at 200 mA cm^{-2} due to its water uptake properties compared to other commercially available ionomers. All experiments used a Sigracet® carbon-based GDE with a 300 nm copper (Cu) layer deposited by physical vapor deposition (PVD) on the microporous layer, followed by spray-coating with an additional catalyst-ionomer layer (3.5 mg Cu cm^{-2}) containing Cu nanoparticles and a trimethyl ammonia poly(phenol oxide) anion exchange ionomer of ionomer–catalyst (I : C) ratio of 0.3. All electrochemical experiments were performed in a 5 cm^2 zero-gap electrolyzer heated to 40 °C, fed with 40 °C pre-heated, humidified CO_2 gas to the cathode, and room temperature 0.5 M KOH from a 5 L anolyte reservoir at the anode. Gas flow rates of the experiments were all monitored through a mass flow meter. All data sets used a steady-state, non-precipitation flow rate to calculate the faradaic efficiency (FE) of gas products. We identify precipitation events indirectly by monitoring fluctuations in the gas chromatography data alongside decreases in the mass flow rate. Both signals indicate partial salt blockages in the flow fields, which lead to unsteady gas flow rates reaching the gas chromatograph.

Using our previously optimized I : C ratio of 0.3, we identified the temporal failure of a precipitation event, of our electrolyzer at 2.5 hours when applying a steady-state current of 200 mA cm^{-2}.[22,23] We were able to identify precipitation as the root-cause of failure due to the changes observed as a drop in flow rate at our mass flow meter. We observed a steady decrease in mass flow downstream of the gas chromatograph, indicating blockage within the flow field. This was confirmed upon dismantling the electrolyzer, where precipitates were found in the flow channels (Fig. S1). To demonstrate the blockages through our GC data, we maintained the steady-state CO_2 flow rate for calculating our gas product selectivity. Maintaining a constant gas flow rate during our calculations allows individual data points to fluctuate and can result in the total faradaic yield exceeding 100%. When combined with mass flow meter readings, this serves as an online indicator of precipitation in this study (Fig. S2).

We observed that continuous electrolyzer operation at 200 mA cm^{-2} for approximately 1–2 hours resulted in precipitation and complete blockage of the flow fields (Fig. 2(c)). To mitigate this issue, we systematically investigated the limits of our electrochemical pulsing protocol by sequentially stepping down and stepping up the J_R for 15 minutes, followed by 45 minutes of operation at J_P, and tracked the relative change in ethylene selectivity over time. 15 minutes was chosen as the first J_R because it was the shortest cycle for which we could obtain accurate gas chromatography data, whilst 45 minutes was slightly below the one-hour threshold after which precipitation would be observed. Fig. 2(b) shows the faradaic efficiency for ethylene ($FE_{ethylene}$) while stepping down the J_R from 100 mA cm^{-2} to 30 mA cm^{-2}, whilst Fig. 2(c) shows the $FE_{ethylene}$ when stepping up J_R from 20 mA cm^{-2} to 100 mA cm^{-2}. When progressively stepping up J_R from 10 mA cm^{-2} to 90 mA cm^{-2} over the course of several hours, we observe a low initial $FE_{ethylene}$ of 20% whereas, when progressively stepping down J_R, the initial $FE_{ethylene}$ is 30%. However, during both experiments, the $FE_{ethylene}$ increases throughout the 45 minutes at t_P; we attribute this rise in ethylene selectivity over the course of 45 minutes to a rise in potassium ion (K^+) concentration at the cathode catalyst.[24] The increase in cation transport is due to the co-ion electro-osmotic drag through anion exchange membranes, which is more pronounced at higher current densities.[22,25] Previous studies have demonstrated that increasing the local concentration of alkali cations at the cathode enhances carbon dioxide electro-reduction[26] and facilitates carbon–carbon bond formation on copper catalysts.[26–28] Stepping down J_R from 100 mA cm^{-2} to 20 mA cm^{-2} allows for an initial large accumulation of K^+ at the cathode. In contrast, starting from a low J_R (10–20 mA cm^{-2}) leads to slower accumulation of K^+ at the cathode, delaying the conditions for enhanced ethylene production. The effect of K^+ can be seen through the gradual increase in $FE_{ethylene}$ throughout the step-up experiment. To validate this hypothesis, we conducted two experiments by pulsing the current density between 10–50 mA cm^{-2} and 90–50 mA cm^{-2},

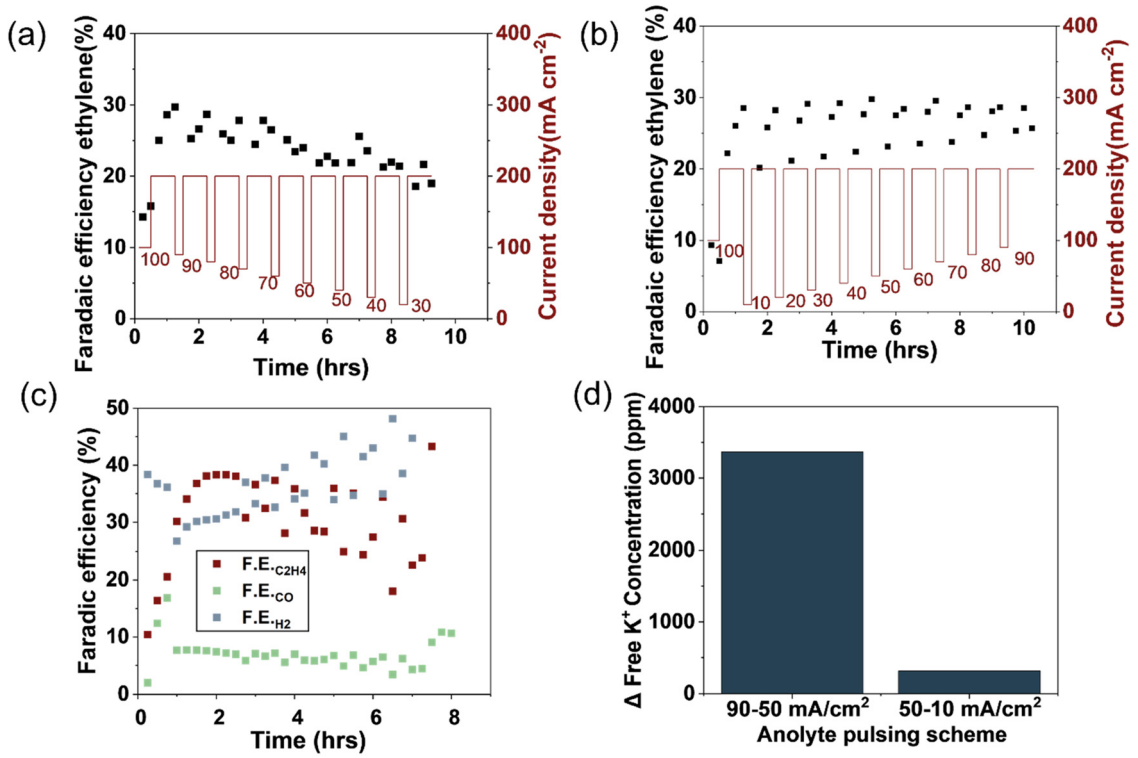

Fig. 2 Faradaic efficiency for ethylene during CO_2 electrolysis with pulsed and constant current at 200 mA cm^{-2}. (a) Faradaic efficiency toward ethylene during pulsed electrochemistry, when progressively increasing J_R (b) and progressively lowering J_R. (c) The line graph indicates the current density. When progressively raising the relaxation current density, the selectivity toward ethylene lags during the first few points after returning to the primary current density, indicating that reaching a steady state takes place over a few minutes of continuous operation. (d) Measurement of the change in potassium ion concentrations during experiments stepping down J_R from 90 to 50 mA cm^{-2} and stepping up J_R from 10 to 50 mA cm^{-2}.

respectively. Free K^+ concentrations were measured using a potassium ion-selective electrode before and after each test.[29] The results revealed a more than tenfold difference in K^+ depletion, with the anolyte showing a ΔK^+ depletion of 5727.13 ppm in the 90–50 mA cm^{-2} test solution compared to 359.27 ppm in the 10–50 mA cm^{-2} solution (Fig. 2d). We do note that the higher K^+ concentration (0.5 M) may lead to significant K^+ crossover due to diffusion in the presence of a Sustainion™ membrane. However, the order of magnitude discrepancy between ΔK^+ from the pulse-up and pulse-down experiments suggests that osmotic-drag is the dominant phenomenon influencing crossover.

Both the step-up and step-down experiments showed that operating for 15 minutes at any of the tested reduced currents (10–100 mA cm^{-2}) extended the electrolyzer lifetime compared to continuous operation at J_P. However, due to the changes in K^+ transport during a step-up or step-down pulse sequence, the effects of cation transport and the specific reduced current densities on the $FE_{ethylene}$ remain convoluted. To isolate the effects of J_R, we performed durability experiments to observe changes in the ethylene selectivity, as a function of J_R, as a proxy for monitoring the onset of precipitation. We chose 100, 50 and 20 mA cm^{-2} as J_R to investigate the boundaries of our initial study and an intermediate current density (Fig. 3(a)). We observe that precipitation does eventually occur when J_R is 100 and 50 mA cm^{-2}, as seen through fluctuations in product selectivity. When J_R is 100 mA cm^{-2} (Fig. S3(a)), we observe variability in $FE_{ethylene}$ for the entire experiment but with fluctuations of rising amplitude occurring after 4 hours. When J_R is 50 mA cm^{-2} (Fig. S3(b)), we observe relatively steady product selectivity, followed by precipitation at 7 hours. We postulate that the enhanced fluctuations observed during the electrochemical pulsing with J_R at 100 mA cm^{-2} are linked to a reduction in water crossover from the anode to the cathode, caused by diminished electro-osmotic drag at current densities lower than the operational current. The decrease in water crossover from anode to cathode, coupled with an intermediate water consumption rate, is likely leading to early precipitation/dissolution events due to a lack of water at the catalyst interface and within the flow field. In contrast, we associate the precipitation occurring at 50 mA cm^{-2} with a depletion of K^+ in our anolyte reservoir. A lower K^+ concentration in the anolyte reduces K^+ crossover to the cathode, thereby decreasing the amount of water that crosses over from the anolyte to the cathode. This gradual decrease in water crossover leads to dehydration and eventual precipitation of carbonate salts at the cathode.

When J_R was reduced to 20 mA cm^{-2}, there is stable $FE_{ethylene}$ for the first 10 hours, followed by a gradual decrease in the 30 and 45-minute gas chromatography measurements post each t_R (Fig. S3(c)). The gradual and uniform drop in ethylene selectivity at the second and third measurements, but not the first, suggests that this reduction in selectivity was due to depletion of K^+ in the system, as opposed to salt precipitation, which

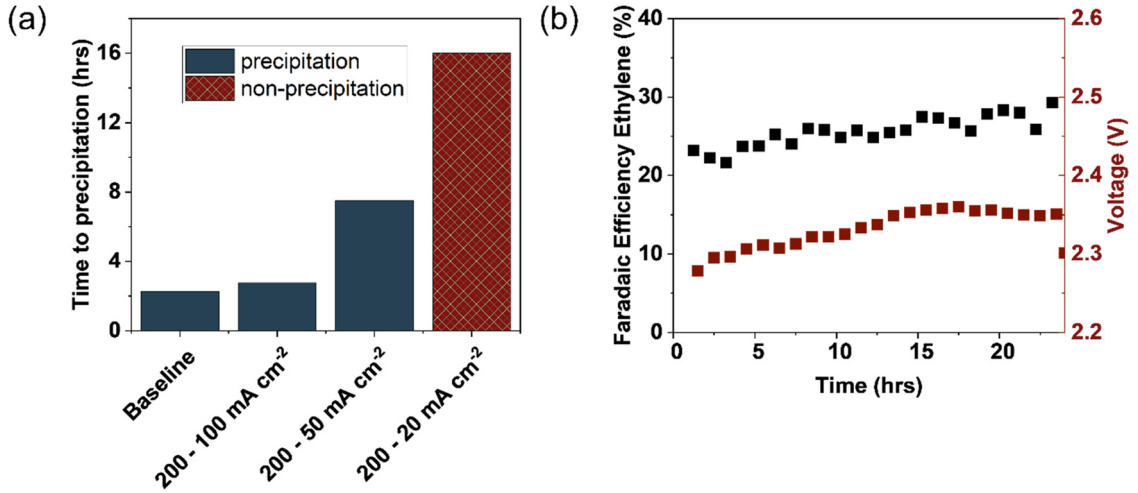

Fig. 3 (a) Comparison of time to precipitate, determined from when CO_2 flow was no longer observed at the outlet of the cell, for the baseline experiment (constant 200 mA cm^{-2} current density), and pulsing protocols with $J_P - J_R$ of 200 − 100 mA cm^{-2}, 200 − 50 mA cm^{-2} and 200 − 20 mA cm^{-2} (b) demonstration of 24 hours of stability using a 200 − 20 mA cm^{-2} pulsed current profile.

would impact all measurements. This hypothesis was tested in a 25-hour experiment (Fig. 3(b), Fig. S4), during which the anolyte reservoir was replaced after 9 hours. The anolyte exchange resulted in a steady increase of $FE_{ethylene}$, suggesting that the introduction of additional K^+ impacts product selectivity; four hours after the anolyte exchange, a similar reduction in $FE_{ethylene}$ was observed, further supporting the hypothesis that K^+ crossover and maintaining a steady-state water flux is an important aspect of this system. Analysis of the anolyte after 15 hours of electrolysis indicates that the pH remains unchanged at pH $>$ 13.5. This result demonstrates the ability to maintain selectivity during electrolysis and avoid precipitation by maintaining appropriate crossover rates of both water and potassium cations. Postmortem analysis of the electrode after 24 hours was not performed due to delamination between the membrane and electrode upon removal from the electrolyzer. However, we do note that previous reports of pulsed currents that remain under cathodic potential do not report changes to the Cu morphology as seen when applying oxidative pulses.

While many pulsing procedures seek to stabilize oxidized copper species to enhance ethylene selectivity, we hypothesize that our low-frequency pulsing protocols primarily regulate the distribution of water and salts. *Operando* X-ray absorption spectroscopy (XAS) studies in flow cells have shown that changes to copper's surface oxidation state, and the corresponding changes in product distribution, occur on timescales of seconds to minutes.[30,31] Recent examples of *operando* XAS in zero-gap systems suggest that the reconstruction towards metallic copper occurs even more rapidly without aqueous electrolyte. Our "rest" pulses are still cathodic current, and thus never allow for the formation of more oxidized copper. During constant-current tests, we observed sudden catastrophic failures rather than gradual changes in selectivity, which correlate with the presence of salt deposits in the flow fields upon cell disassembly. Thus, we focus on elucidating how low-frequency pulsing extends cell lifetime by regulating water distribution.

To test our hypothesis that pulsed currents can prevent salt precipitation and flooding in the cathode, we performed *operando* neutron radiography (NR) experiments.[32–36] Importantly, we believe that the differences in geometric area between NR electrolyzer and our laboratory electrolyzer leads to our NR electrolyzer not fully precipitating as we observed for our laboratory electrolyzer. The decrease in total current (3 cm^2 *vs.* 5 cm^2) leads to a decrease in cation crossover, coupled with identical humidity between both experiments allowing for the 3 cm^2 electrolyzer to keep any K^+ dissolved. Additionally, the NR electrolyzer also has parallel flow fields rather than single serpentine flow fields used for benchmarking, which may affect distribution of CO_2 and humidity through the back of the GDE, leading to slightly different effects. Nonetheless, we expect that the highly different water distributions observed under pulsed *versus* constant current operation are representative of general behavior, with precipitation being delayed rather than entirely suppressed.

After an initial conditioning period (15 minutes at 100 mA cm^{-2}), the cell underwent four cycles of 45 minutes at 200 mA cm^{-2} (J_P) and 15 minutes at 20 mA cm^{-2} (J_R). Using a fresh catalyst and electrolyte, the experiment was repeated at a constant current of 200 mA cm^{-2} for the same duration. The voltage and measured CO_2 at the outlet of the neutron radiography experiments can be found in Fig. S5. Interestingly, the time at J_R (top row of Fig. 4(b)) allowed water transport through the GDE into the flow fields, with subsequent drying during J_P. Despite the wetting of the flow fields, the back of the GDE remained dry throughout due to its hydrophobicity, observed through the less attenuated gap between the membrane and the flow field channels.[36] The pulsed test was also extended to a final 200 mA cm^{-2} pulse, where the flow fields and electrode were relatively dry again (Fig. S6). Additionally, there were no signs of salt formation during the postmortem inspection.

In contrast, in the constant current test (bottom row of Fig. 4(b)), water permeates through the GDE without reaching

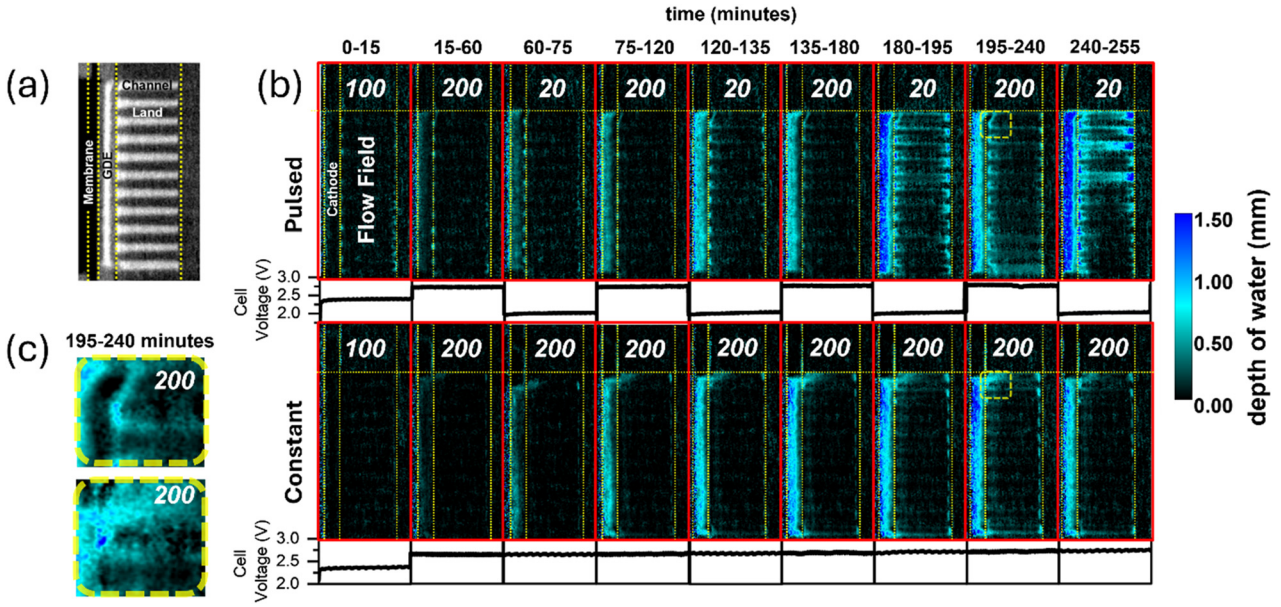

Fig. 4 (a) Transmission neutron radiograph (cropped to the cathode area) of the electrolyzer before electrolyzer operation. (b) *Operando* neutron radiograph. The baseline radiograph was taken with continuous anolyte flow, continuous CO_2 flow without humidification, steady temperature at 40 °C, and before applying an electrical current. (c) Inset of neutron radiographs in dashed yellow squares from 4b – top: pulsed, bottom: constant current.

the flow field channels until it begins to flood near the inlet at the end of the test after about 200 minutes. This is observed by the increase in intensity at the top right of the constant current radiograph from 195–240 minutes, a feature which is not observed in the radiograph with the same timestamp in the pulsed current test. This increase in intensity at the inlet may result from either water accumulation or salt precipitation, although precipitation would likely have to be from potassium bicarbonate (rather than the less soluble carbonate salt) as carbonate does not strongly attenuate neutrons. During J_P, the drying of the GDE could be a result of the increase in water consumption due to the increase in current density.[37] The reduced rate of liquid product production allows excess water to pass through the GDE, thereby alleviating product build-up and water accumulation. These data suggest that water accumulation in the flow channels does not necessarily induce cathode flooding; rather, flooding occurs only when the GDL reaches maximum saturation throughout the entire thickness. Maximum saturation is dependent on the hydrophobicity of the GDL material. Carbon-based Toray and Freudenberg -comparable to Sigracet - have been shown to achieve maximum saturation of 45–50%.[38,39]

Collectively, these electrochemical, gas composition, and radiographic measurements suggest that the applied pulsed-current protocol enables dynamic re-stabilization by allowing water to redistribute and flush through the GDE. The hypothesized mechanism of regeneration is summarized in Fig. 1a. The relaxation period at low current density allows for a "flushing" of the back of the catalyst from a combination of water transport through the GDE, diffusion, and humidified CO_2 at the inlet to remove precipitated salts. During J_R the decrease in water consumption from lower current densities allows for mixing of liquid products such as ethanol into the water, which can decrease in surface tension of the water and allow the mixture to rapidly diffuse away from the catalyst surface. Once the current returns to J_P water is more rapidly consumed at the higher current densities, but more importantly organic byproducts are removed from the catalyst layer allowing the hydrophobic microporous layer to promote CO_2 reduction as opposed to HER.[40,41] Thus, the pulses allow for balancing of the amount of water in the GDE, while also periodically removing precipitated salts and organic byproducts, both of which are essential for high efficiency, long duration electrochemical ethylene production. Using *operando* neutron imaging we were able to validate our hypothesis about the role of pulsing on water management in the catalyst layer which facilitated doubling the durability of the electrolyzer.

Conclusions

In this study, we enhanced the understanding of how low-frequency pulsing at low current density facilitates the removal of excess water and mitigates salt accumulation. We also identified key considerations for designing an effective electrochemical pulsing protocol. Given the unique and specific chemical and electrochemical dynamics of each CO_2RR setup, it is vital to account for all potential interactions involved, including the choice of membrane, alkaline salt, and the type of electrolyzer. This ensures the creation of a pulsing protocol tailored to minimize the rate and nature of precipitation in specific configurations. Our findings establish a flexible framework that can be adapted across different setups, ultimately enhancing the longevity and efficiency of electrolyzers. Further refinement of pulsing strategies using *operando* observation of the system as a guide,

alongside monitoring the anolyte's free K^+ concentration and periodically replacing anolyte could provide a pathway to long-term stable operation of zero-gap CO_2 to ethylene electrolyzers.

Author contributions

M. M and M. G. conceptualized the project and designed the methodology. M. M, M. G., and D. R. wrote the original draft M. M., M. G. D. R. carried out all electrochemical experiments, M. M., M. G, D. R. and A. W. analyzed data, contributed to the discussion, and prepared the manuscript. J. D., M. T., M. G., D. R., J. L. collected the neutron radiography data. P. A. B, P. T. C. H., S. B., and E. D. edited the manuscript. E. K. and A. C. prepared the gas diffusion electrodes. M. G, E. D, S. B, C. H supervised the project.

Conflicts of interest

The authors have no conflicts to declare.

Data availability

The data supporting this article have been included as part of the supplementary information. Supplementary information (SI) is available. See DOI: https://doi.org/10.1039/d6ey00012f.

Acknowledgements

This material is based upon work supported by the U.S. Department of Energy's Office of Energy Efficiency and Renewable Energy (EERE) under the Advanced Manufacturing Office (AMO) funding opportunity announcement DE-FOA-0002252 in partnership with Siemens Energy SE and Total Energies SE under CRADA TC02449, and Lawrence Livermore Laboratory Directed Research and Development funding under project 22-SI-006. M.M., M.G., D.R., J.D., M.T., E.K., A.W., E.D., S.B., C.H. contributed under the auspices of the US Department of Energy by Lawrence Livermore National Laboratory under contract DE-AC52-07NA27344 with release number IM: LLNL-JRNL-2012865. This work is based on experiments (beamtime proposal No. 20240011) performed at the Swiss spallation neutron source SINQ, Paul Scherrer Institute, Villigen, Switzerland. Funding for the neutron radiography experiments and data analysis was provided by U.S. Department of Energy Office of Energy Efficiency and Renewable Energy Bioenergy Technologies Office. The U.S. Government retains and the publisher, by accepting the article for publication, acknowledges that the U.S. Government retains a nonexclusive, paid-up, irrevocable, worldwide license to publish or reproduce the published form of this work, or allow others to do so, for U.S. Government purposes.

References

1 Y. Yao, T. Shi, W. Chen, J. Wu, Y. Fan, Y. Liu, L. Cao and Z. Chen, A Surface Strategy Boosting the Ethylene Selectivity for CO2 Reduction and in Situ Mechanistic Insights, *Nat. Commun.*, 2024, **15**(1), 1257, DOI: 10.1038/s41467-024-45704-2.

2 W. Li, Z. Yin, Z. Gao, G. Wang, Z. Li, F. Wei, X. Wei, H. Peng, X. Hu, L. Xiao, J. Lu and L. Zhuang, Bifunctional Ionomers for Efficient Co-Electrolysis of CO2 and Pure Water towards Ethylene Production at Industrial-Scale Current Densities, *Nat. Energy*, 2022, **7**(9), 835–843, DOI: 10.1038/s41560-022-01092-9.

3 L. Yuan, S. Zeng, X. Zhang, X. Ji and S. Zhang, Advances and Challenges of Electrolyzers for Large-Scale CO2 Electroreduction, *Mater. Rep. Energy*, 2023, **3**(1), 100177, DOI: 10.1016/j.matre.2023.100177.

4 D. Wakerley, S. Lamaison, J. Wicks, A. Clemens, J. Feaster, D. Corral, S. A. Jaffer, A. Sarkar, M. Fontecave, E. B. Duoss, S. Baker, E. H. Sargent, T. F. Jaramillo and C. Hahn, Gas Diffusion Electrodes, Reactor Designs and Key Metrics of Low-Temperature CO2 Electrolysers, *Nat. Energy*, 2022, **7**(2), 130–143, DOI: 10.1038/s41560-021-00973-9.

5 I. E. L. Stephens, K. Chan, A. Bagger, S. W. Boettcher, J. Bonin, E. Boutin, A. K. Buckley, R. Buonsanti, E. R. Cave, X. Chang, S. W. Chee, A. H. M. Silva, P. da; Luna, O. de; Einsle, B. Endrődi, M. Escudero-Escribano, J. V. F. Araujo, M. C. de; Figueiredo, C. Hahn, K. U. Hansen, S. Haussener, S. Hunegnaw, Z. Huo, Y. J. Hwang, C. Janáky, B. S. Jayathilake, F. Jiao, Z. P. Jovanov, P. Karimi, M. T. M. Koper, K. P. Kuhl, W. H. Lee, Z. Liang, X. Liu, S. Ma, M. Ma, H.-S. Oh, M. Robert, B. R. Cuenya, J. Rossmeisl, C. Roy, M. P. Ryan, E. H. Sargent, P. Sebastián-Pascual, B. Seger, L. Steier, P. Strasser, A. S. Varela, R. E. Vos, X. Wang, B. Xu, H. Yadegari and Y. Zhou, Roadmap on Low Temperature Electrochemical CO2 Reduction, *J. Phys. Energy*, 2022, **4**(4), 042003, DOI: 10.1088/2515-7655/ac7823.

6 U. O. Nwabara, E. R. Cofell, S. Verma, E. Negro and P. J. A. Kenis, Durable Cathodes and Electrolyzers for the Efficient Aqueous Electrochemical Reduction of CO2, *ChemSusChem*, 2020, **13**(5), 855–875, DOI: 10.1002/cssc.201902933.

7 R. Casebolt, K. Levine, J. Suntivich and T. Hanrath, Pulse Check: Potential Opportunities in Pulsed Electrochemical CO2 Reduction, *Joule*, 2021, **5**(8), 1987–2026, DOI: 10.1016/j.joule.2021.05.014.

8 S. Nitopi, E. Bertheussen, S. B. Scott, X. Liu, A. K. Engstfeld, S. Horch, B. Seger, I. E. L. Stephens, K. Chan, C. Hahn, J. K. Nørskov, T. F. Jaramillo and I. Chorkendorff, Progress and Perspectives of Electrochemical CO2 Reduction on Copper in Aqueous Electrolyte, *Chem. Rev.*, 2019, **119**(12), 7610–7672, DOI: 10.1021/acs.chemrev.8b00705.

9 R. M. Arán-Ais, F. Scholten, S. Kunze, R. Rizo and B. Roldan Cuenya, The Role of in Situ Generated Morphological Motifs and Cu(I) Species in C2+ Product Selectivity during CO2 Pulsed Electroreduction, *Nat. Energy*, 2020, **5**(4), 317–325, DOI: 10.1038/s41560-020-0594-9.

10 K. W. Kimura, K. E. Fritz, J. Kim, J. Suntivich, H. D. Abruña and T. Hanrath, Controlled Selectivity of CO2 Reduction on Copper by Pulsing the Electrochemical Potential, *ChemSusChem*, 2018, **11**(11), 1781–1786, DOI: 10.1002/cssc.201800318.

11 J. M. Strain, S. Gulati, S. Pishgar and J. M. Spurgeon, Pulsed Electrochemical Carbon Monoxide Reduction on Oxide-Derived Copper Catalyst, *ChemSusChem*, 2020, **13**(11), 3028–3033, DOI: 10.1002/cssc.202000464.

12 J. C. Bui, C. Kim, A. Z. Weber and A. T. Bell, Dynamic Boundary Layer Simulation of Pulsed CO_2 Electrolysis on a Copper Catalyst, *ACS Energy Lett.*, 2021, 1181–1188, DOI: 10.1021/acsenergylett.1c00364.

13 L.-C. Weng, A. T. Bell and A. Z. Weber, A Systematic Analysis of Cu-Based Membrane-Electrode Assemblies for CO2 Reduction through Multiphysics Simulation, *Energy Environ. Sci.*, 2020, **13**(10), 3592–3606, DOI: 10.1039/D0EE01604G.

14 A. Engelbrecht, C. Uhlig, O. Stark, M. Hämmerle, G. Schmid, E. Magori, K. Wiesner-Fleischer, M. Fleischer and R. Moos, On the Electrochemical CO2 Reduction at Copper Sheet Electrodes with Enhanced Long-Term Stability by Pulsed Electrolysis, *J. Electrochem. Soc.*, 2018, **165**(15), J3059, DOI: 10.1149/2.0091815jes.

15 J. Kok, J. de Ruiter, W. van der Stam and T. Burdyny, Interrogation of Oxidative Pulsed Methods for the Stabilization of Copper Electrodes for CO2 Electrolysis, *J. Am. Chem. Soc.*, 2024, **146**(28), 19509–19520, DOI: 10.1021/jacs.4c06284.

16 Y. Xu, J. P. Edwards, S. Liu, R. K. Miao, J. E. Huang, C. M. Gabardo, C. P. O'Brien, J. Li, E. H. Sargent and D. Sinton, Self-Cleaning CO_2 Reduction Systems: Unsteady Electrochemical Forcing Enables Stability, *ACS Energy Lett.*, 2021, **6**(2), 809–815, DOI: 10.1021/acsenergylett.0c02401.

17 D. G. Wheeler, B. A. W. Mowbray, A. Reyes, F. Habibzadeh, J. He and C. P. Berlinguette, Quantification of Water Transport in a CO2 Electrolyzer, *Energy Environ. Sci.*, 2020, **13**(12), 5126–5134, DOI: 10.1039/D0EE02219E.

18 *Unveiling transport mechanisms of cesium and water in operando zero-gap CO2 electrolyzers - ScienceDirect*. https://www.sciencedirect.com/science/article/pii/S2542435124001107?via%3Dihub (accessed 2025-06-11).

19 S. Garg, Q. Xu, A. B. Moss, M. Mirolo, W. Deng, I. Chorkendorff, J. Drnec and B. Seger, How Alkali Cations Affect Salt Precipitation and CO2 Electrolysis Performance in Membrane Electrode Assembly Electrolyzers, *Energy Environ. Sci.*, 2023, **16**(4), 1631–1643, DOI: 10.1039/D2EE03725D.

20 H. W. Shafaque, C. Lee, K. F. Fahy, J. K. Lee, J. M. LaManna, E. Baltic, D. S. Hussey, D. L. Jacobson and A. Bazylak, Boosting Membrane Hydration for High Current Densities in Membrane Electrode Assembly CO2 Electrolysis, *ACS Appl. Mater. Interfaces*, 2020, **12**(49), 54585–54595, DOI: 10.1021/acsami.0c14832.

21 L. Bohn, J. Häberlein, F. Brendel, L. Metzler, L. Helfen, A. Tengattini, C. Klose, S. Vierrath and J. Disch, High-Resolution Neutron Imaging of Water Transport in CO2 Electrolysis during Pulsed Operation, *ACS Energy Lett.*, 2025, **10**(2), 975–981, DOI: 10.1021/acsenergylett.4c03003.

22 M. Goldman, A. Prajapati, N. R. Cross, A. Clemens, A. T. Chu, L. Gutierrez, M. Marufu, E. Krall, V. Ehlinger, T. Moore, E. B. Duoss, S. E. Baker and C. Hahn, Designing Ionomers to Control Water Content for Low-Voltage Ethylene Production from CO2 Electrolysis, *Chem. Catal.*, 2025, **5**(11), 101497, DOI: 10.1016/j.checat.2025.101497.

23 Z. Feng, P. O. Esteban, G. Gupta, D. A. Fulton and M. Mamlouk, Highly Conductive Partially Cross-Linked Poly(2,6-Dimethyl-1,4-Phenylene Oxide) as Anion Exchange Membrane and Ionomer for Water Electrolysis, *Int. J. Hydrogen Energy*, 2021, **46**(75), 37137–37151, DOI: 10.1016/j.ijhydene.2021.09.014.

24 N. Chang, T. Li, R. Li, S. Wang, Y. Yin, H. Zhang and X. Li, An Aqueous Hybrid Electrolyte for Low-Temperature Zinc-Based Energy Storage Devices, *Energy Environ. Sci.*, 2020, **13**(10), 3527–3535, DOI: 10.1039/D0EE01538E.

25 F. Habibzadeh, P. Mardle, N. Zhao, H. D. Riley, D. A. Salvatore, C. P. Berlinguette, S. Holdcroft and Z. Shi, Ion Exchange Membranes in Electrochemical CO2 Reduction Processes, *Electrochem. Energy Rev.*, 2023, **6**(1), 26, DOI: 10.1007/s41918-023-00183-9.

26 J. Resasco, L. D. Chen, E. Clark, C. Tsai, C. Hahn, T. F. Jaramillo, K. Chan and A. T. Bell, Promoter Effects of Alkali Metal Cations on the Electrochemical Reduction of Carbon Dioxide, *J. Am. Chem. Soc.*, 2017, **139**(32), 11277–11287, DOI: 10.1021/jacs.7b06765.

27 S. Ringe, E. L. Clark, J. Resasco, A. Walton, B. Seger, A. T. Bell and K. Chan, Understanding Cation Effects in Electrochemical CO2 Reduction, *Energy Environ. Sci.*, 2019, **12**(10), 3001–3014, DOI: 10.1039/C9EE01341E.

28 G. A. El-Nagar, F. Haun, S. Gupta, S. Stojkovikj and M. T. Mayer, Unintended Cation Crossover Influences CO2 Reduction Selectivity in Cu-Based Zero-Gap Electrolysers, *Nat. Commun.*, 2023, **14**(1), 2062, DOI: 10.1038/s41467-023-37520-x.

29 F. J. Vidal-Iglesias, J. Solla-Gullón, A. Rodes, E. Herrero and A. Aldaz, Understanding the Nernst Equation and Other Electrochemical Concepts: An Easy Experimental Approach for Students, *J. Chem. Educ.*, 2012, **89**(7), 936–939, DOI: 10.1021/ed2007179.

30 J. Timoshenko, A. Bergmann, C. Rettenmaier, A. Herzog, R. M. Arán-Ais, H. S. Jeon, F. T. Haase, U. Hejral, P. Grosse, S. Kühl, E. M. Davis, J. Tian, O. Magnussen and B. Roldan Cuenya, Steering the Structure and Selectivity of CO2 Electroreduction Catalysts by Potential Pulses, *Nat. Catal.*, 2022, **5**(4), 259–267, DOI: 10.1038/s41929-022-00760-z.

31 T. S. Chou, C. C. Chang, W. Y. Yu, C. L. Dong, J. J. Velasco-Vélez, C. H. Chuang, L. C. Chen, J. F. Lee, J. M. Chen and H. L. Wu, Controlling the Oxidation State of the Cu Electrode and Reaction Intermediates for Electrochemical CO_2 Reduction to Ethylene, *J. Am. Chem. Soc.*, 2020, **142**(6), 2857–2867, DOI: 10.1021/jacs.9b11126.

32 E. H. Lehmann, P. Vontobel and L. Wiezel, Properties of the Radiography Facility Neutra at Sinq and Its Potential for Use as European Reference Facility, *Nondestruct. Test. Eval.*, 2001, **16**(2–6), 191–202, DOI: 10.1080/10589750108953075.

33 P. Boillat, G. Frei, E. H. Lehmann, G. G. Scherer and A. Wokaun, Neutron Imaging Resolution Improvements Optimized for Fuel Cell Applications, *Electrochem. Solid-State Lett.*, 2010, **13**(3), B25, DOI: 10.1149/1.3279636.

34 E. H. Lehmann, P. Vontobel and L. Wiezel, Properties of the Radiography Facility Neutra at Sinq and Its Potential for Use

as European Reference Facility, *Nondestruct. Test. Eval.*, 2001, **16**(2–6), 191–202, DOI: 10.1080/10589750108953075.

35 P. Boillat, C. Carminati, F. Schmid, C. Grünzweig, J. Hovind, A. Kaestner, D. Mannes, M. Morgano, M. Siegwart, P. Trtik, P. Vontobel and E. H. Lehmann, Chasing Quantitative Biases in Neutron Imaging with Scintillator-Camera Detectors: A Practical Method with Black Body Grids, *Opt. Express*, 2018, **26**(12), 15769–15784, DOI: 10.1364/OE.26.015769.

36 A. Iranzo, P. Boillat and F. Rosa, Validation of a Three Dimensional PEM Fuel Cell CFD Model Using Local Liquid Water Distributions Measured with Neutron Imaging, *Int. J. Hydrogen Energy*, 2014, **39**(13), 7089–7099, DOI: 10.1016/j.ijhydene.2014.02.115.

37 J. Disch, L. Bohn, S. Koch, M. Schulz, Y. Han, A. Tengattini, L. Helfen, M. Breitwieser and S. Vierrath, High-Resolution Neutron Imaging of Salt Precipitation and Water Transport in Zero-Gap CO2 Electrolysis, *Nat. Commun.*, 2022, **13**(1), 6099, DOI: 10.1038/s41467-022-33694-y.

38 M. A. Rahman, M. Sarker, F. Mojica and P.-Y. A. Chuang, A Physics-Based 1-D PEMFC Model for Simulating Two-Phase Water Transport in the Electrode and Gas Diffusion Media, *Appl. Energy*, 2022, **316**, 119101, DOI: 10.1016/j.apenergy.2022.119101.

39 *The interactive effect of heat and mass transport on water condensation in the gas diffusion layer of a proton exchange membrane fuel cell - ScienceDirect*. https://www.sciencedirect.com/science/article/pii/S0378775320314142 (accessed 2025-11-14).

40 Choice—Flooded by Success: On the Role of Electrode Wettability in CO2 Electrolyzers That Generate Liquid Products, ed Leonard, M. E.; Orella, M. J.; Aiello, N.; Román-Leshkov, Y.; Forner-Cuenca, A.; Brushett, F. R., *Journal of the Electrochemical Society*, 2020, vol. 167 (12), p. 124521. , DOI: 10.1149/1945-7111/abaa1a.

41 D. Corral, J. T. Feaster, S. Sobhani, J. R. DeOtte, D. U. Lee, A. A. Wong, J. Hamilton, V. A. Beck, A. Sarkar, C. Hahn, T. F. Jaramillo, S. E. Baker and E. B. Duoss, Advanced Manufacturing for Electrosynthesis of Fuels and Chemicals from CO2, *Energy Environ. Sci.*, 2021, **14**(5), 3064–3074, DOI: 10.1039/D0EE03679J.